nature materials

ARTICLES

PUBLISHED ONLINE: 1 AUGUST 2016 | DOI: 10.1038/NMAT4708

Electrochemical stiffness in lithium-ion batteries

Hadi Tavassol[1†], Elizabeth M. C. Jones[2,3†], Nancy R. Sottos[3,4*] and Andrew A. Gewirth[1*]

Although lithium-ion batteries are ubiquitous in portable electronics, increased charge rate and discharge power are required for more demanding applications such as electric vehicles. The high-rate exchange of lithium ions required for more power and faster charging generates significant stresses and strains in the electrodes that ultimately lead to performance degradation. To date, electrochemically induced stresses and strains in battery electrodes have been studied only individually. Here, a new technique is developed to probe the chemomechanical response of electrodes by calculating the electrochemical stiffness via coordinated *in situ* stress and strain measurements. We show that dramatic changes in electrochemical stiffness occur due to the formation of different graphite–lithium intercalation compounds during cycling. Our analysis reveals that stress scales proportionally with the lithiation/delithiation rate and strain scales proportionally with capacity (and inversely with rate). Electrochemical stiffness measurements provide new insights into the origin of rate-dependent chemomechanical degradation and the evaluation of advanced battery electrodes.

Lithium-ion batteries are electrochemical energy storage devices in which lithium ions are cycled between two electrodes. The rate capability of electrodes is limited in part by dramatic mechanical changes that occur when lithium ions are inserted and removed from the electrodes[1,2]. Interaction of lithium ions with electrode materials during battery charging and discharging generates internal pressure (stress) within the electrode structure[3–8]. Generally, stress measurements in electrochemical systems report on interactions occurring from the sub-monolayer to the bulk of electrode materials[9]. In battery electrodes, lithium-ion insertion effects dominate the stress response of the system. Electrode materials develop compressive stress during lithiation (Fig. 1a). During delithiation, this compressive stress is released, where the mechanism of lithium-ion exchange (for example, intercalation such as in graphitic electrodes[6,8,10,11], formation of intermetallic compounds such as in silicon-based electrodes[5,7] or alloying such as in tin-based electrodes[3]) controls the stress relief response. In addition to stress generation, interaction of lithium ions with electrodes induces volumetric changes and displacements (strain) of the active material in the electrode (Fig. 1b). Electrode materials expand during lithiation, while contraction of the electrode occurs when lithium ions are removed. X-ray spectroscopy techniques[12,13] and direct imaging methods such as transmission electron microscopy[14,15] and atomic force microscopy[16–18] provide detailed information about electrode deformation at the nanoscale. At the macroscale, deformation of porous composite electrodes has been studied via X-ray tomography[12,13] and digital image correlation[19,20].

The electrochemically induced stresses and strains in battery electrodes become more significant during high-rate charging and discharging[21–23]. Strain analysis of composite electrode materials has revealed that lithiation and delithiation occur through heterogeneous regimes within individual particles of active material or across the entire composite electrode[13,24–26]. Such heterogeneities are even more acute in high-rate exchange of lithium ions and cause sharp stress and strain gradients that ultimately lead to chemical and physical degradation of the electrodes[13,21,27]. Although the kinetics of lithium diffusion in graphite anodes has been studied by electrochemical methods such as impedance spectroscopy[21,28–30], the influence of kinetics effects on stress and strain development is not established.

As stress and strain development in lithium-ion battery electrodes during electrochemical cycling have been studied only individually, the relative contributions of stress and strain to battery performance/degradation in graphite or other battery materials have remained unknown. In this work, we combine *in situ* stress and strain measurements of graphite composite electrodes during electrochemical cycling to calculate an electrochemical stiffness of the electrodes. In contrast to the elastic stiffness constants (for example, Young's modulus), the electrochemical stiffness reported here is a measure of the potential or capacity dependence of the stress and strain responses of the electrodes. We show that tracking changes in the electrochemical stiffness provides new insights into the effects of individual phase changes on the mechanical responses of electrodes as well as insight into kinetic limitations on lithium insertion and removal from the host material. This novel approach offers a new analytical tool for interrogating advanced battery materials, enabling the design and assessment of high-power and high-rate battery materials.

Electrochemical stiffness

We define the electrochemical stiffness, k, as the ratio of an incremental change in stress, $\partial(\Delta\sigma)$, induced by insertion of lithium into a constrained electrode compared with the corresponding incremental change in strain, $\partial(\varepsilon)$, induced by the same lithium insertion in an unconstrained electrode:

$$k_i = \left.\frac{\partial(-\Delta\sigma)}{\partial\varepsilon}\right|_i \tag{1}$$

where i is either the electrode potential, E, or the electrode capacity, Q. The methodology used to link independent but coordinated stress and strain measurements and to compute the electrochemical

[1]Department of Chemistry, University of Illinois at Urbana-Champaign, Urbana, Illinois 61801, USA. [2]Department of Mechanical Science and Engineering, University of Illinois at Urbana-Champaign, Urbana, Illinois 61801, USA. [3]Beckman Institute of Science and Technology, University of Illinois at Urbana-Champaign, Urbana, Illinois 61801, USA. [4]Department of Material Science and Engineering, University of Illinois at Urbana-Champaign, Urbana, Illinois 61801, USA. †These authors contributed equally to this work. *e-mail: n-sottos@illinois.edu; agewirth@illinois.edu

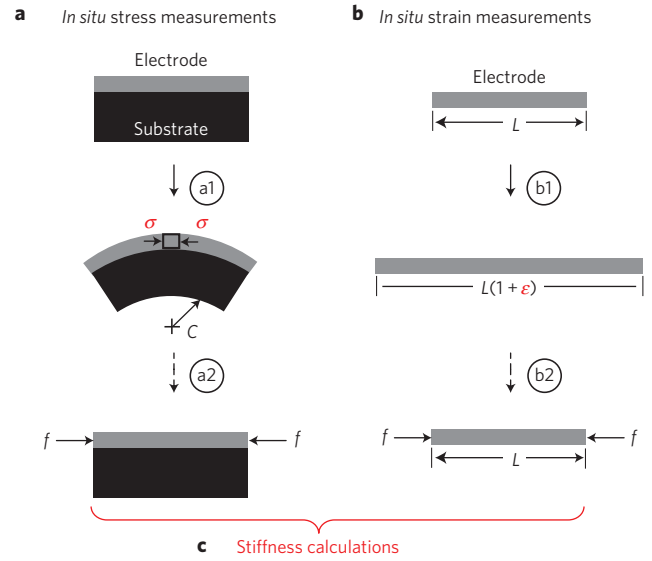

Figure 1 | Methodology for electrochemical stiffness calculations. **a**, Schematic of *in situ* stress measurements. An electrode with an unknown stress state is attached to a substrate. During lithiation, the substrate constrains the free expansion of the electrode, so a change in stress, $\Delta\sigma$, develops in the electrode, resulting in a curvature, C, of the substrate (step a1). A conceptual external force, f, then compresses the electrode to remove the curvature (step a2). **b**, Schematic of *in situ* strain measurements. An unconstrained electrode with characteristic size L undergoes free expansion during lithiation, generating a strain of ε (step b1). The same conceptual external force, f, then compresses the electrode to its original size (step b2). **c**, The electrodes at the end of the steps a2 and b2 have the same size and stress state, and are viewed as the same electrode for the purposes of stiffness calculations.

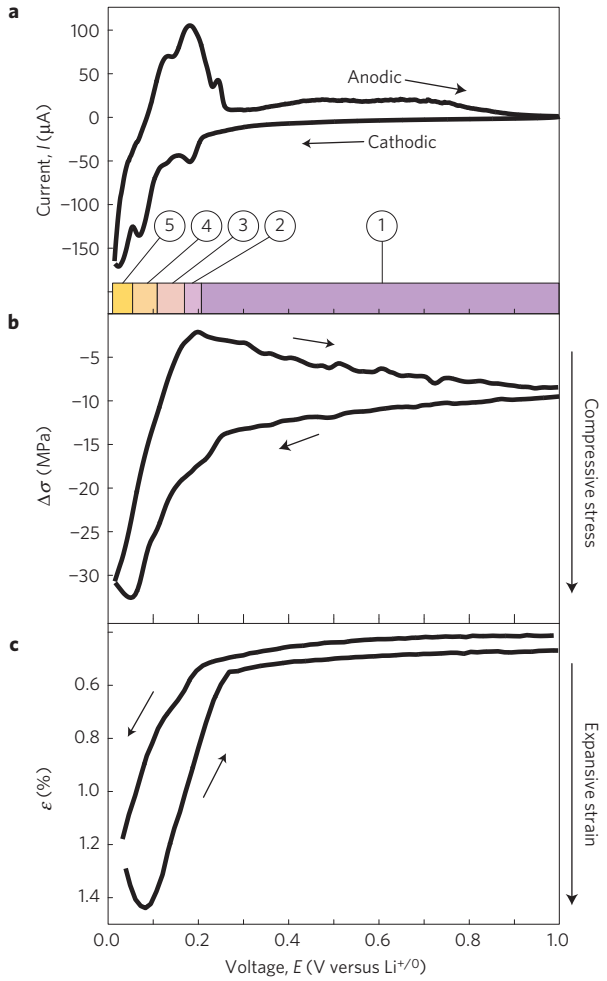

Figure 2 | Potential-dependent electrode response during cyclic voltammetry. a–c, Third-cycle cyclic voltammetry at 25 μV s^{-1} (from stress experiment) (**a**) with corresponding stress (**b**) and strain (**c**) measurements of a graphite anode. The coloured regions in **a** correspond to phase transitions between graphite–lithium intercalation compounds during the cathodic sweep: 1, formation of dilute stage I; 2, dilute stage I to stage IV; 3, stage IV to stage III to dilute stage II; 4, dilute stage II to stage II; 5, stage II to stage I.

stiffness of lithium-ion battery electrodes is illustrated in Fig. 1. In cyclic voltammetry, where electrode potential is the independent variable, the potential-dependent stiffness, k_E, is calculated. In galvanostatic cycling, where electrode capacity is the independent variable, the capacity-dependent stiffness, k_Q, is calculated. The negative sign in the numerator is included to rectify the negative (compressive) stress with the positive (expansive) strain that develop in the electrodes during lithiation. The stress and strain are both dependent variables of electrode potential and capacity. Therefore, the reported electrochemical stiffness values provide a measure of the relative effects of stress compared with strain at a particular point during electrochemical cycling, which is different from the traditional definition of stiffness as a material property such as Young's modulus.

Stress and strain development

In situ stress and strain measurements of graphite composite electrodes were performed in coordinated experiments using the methodologies shown in Fig. 1. The third cycle of cyclic voltammetry and the corresponding stress and strain measurements of graphite composite electrodes are shown in Fig. 2. The compressive stress of about −9.5 MPa and expansive strain of about 0.41% at the start of the cycle (1.0 V) is due to the non-recoverable stress and strain generated during the first two cycles. The irreversible electrode responses are primarily attributed to the irreversible electrochemical reactions that occur during the formation of the solid electrolyte interphase[4,5,19,31–33]. During the cathodic sweep between 1.0 V and 0.3 V, the current is primarily due to the lithiation of disordered carbon black and early lithiation of graphite[34] as well as continued solid electrolyte interphase formation[31,35,36]. In this voltage region, a small compressive stress develops in the constrained electrode, and the unconstrained electrode expands slightly. At more negative potentials (about 0.3 V–0.01 V), the voltammetry shows features corresponding to the phase transitions between distinct graphite–lithium intercalation compounds[36,37], which are discussed further in the Supplementary Information. Stages of intercalation compounds are demarcated by the number of graphite layers associated with each layer of intercalated lithium[38,39]. The formation of intercalation compounds in this lower voltage region results in a rapid increase and changes in the rate of stress and strain development. During the anodic sweep, the compressive stress is relieved and the electrode contracts. The electrode response during the anodic sweep is further discussed in the Supplementary Information.

Potential-dependent mechanical response

The independent stress and strain values from the third cycle of cyclic voltammetry are coordinated at each potential and plotted in Fig. 3a. Changes in the slope result from differences in the development of stress and strain as different intercalation compounds form during lithiation and delithiation of the graphite electrode. The potential-dependent stiffness, k_E, calculated as the slope of the

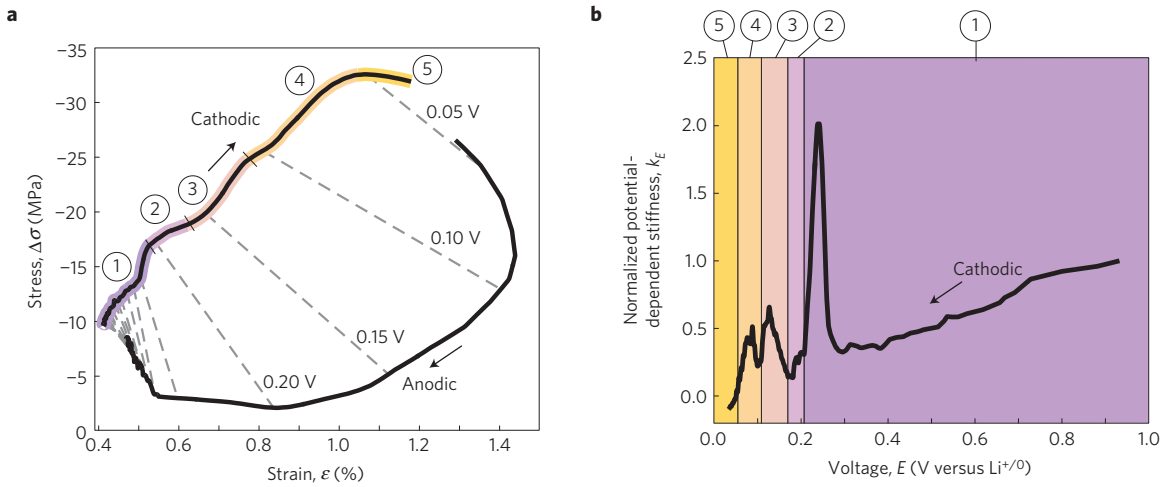

Figure 3 | Coordination of stress and strain measurements and calculation of the electrochemical stiffness. a, The stress and strain responses from the third cycle of cyclic voltammetry at 25 μV s^{-1} (Fig. 2), coordinated at each potential value. The dashed lines represent contours of constant potential in increments of 0.05 V versus $Li^{+/0}$. **b**, Potential-dependent stiffness variations of the electrode during the cathodic sweep of cyclic voltammetry. The *y* axis is normalized with respect to the stiffness value at the beginning of the cycle. Absolute values of the stiffness are presented in the Supplementary Information. The coloured regions correspond to phase transitions between graphite–lithium intercalation compounds: 1, formation of dilute stage I; 2, dilute stage I to stage IV; 3, stage IV to stage III to dilute stage II; 4, dilute stage II to stage II; 5, stage II to stage I.

stress versus strain curve (equation (1)), is reported in Fig. 3b. At the beginning of the cathodic sweep, the electrode exhibits an initially stiff response caused by the immediate development of stress as the first few lithium ions are intercalated into the graphite with minimal corresponding strain development. As the formation of the dilute stage I graphite–lithium intercalation compound progresses (through approximately 0.3 V), strain develops at a faster rate once enough ions are inserted to cause an appreciable increase in graphite layer spacing. This later strain increase causes a corresponding decrease in stiffness of the electrode.

As potential is swept to more negative values, a sharp oscillation in the stiffness occurs at approximately 0.24 V, just before the transition between the disordered dilute stage I compound and the first ordered stage IV compound. At more negative potentials, two additional oscillations in the stiffness are observed at approximately 0.13 V and 0.08 V as high-lithium-content, ordered intercalation compounds are formed. Surprisingly, the increase in stiffness just before the dilute stage I to stage IV transition (0.24 V) is the most intense oscillation during lithiation of the graphitic anodes. This observation is consistent with *in situ* X-ray diffraction analyses, which show that formation of low-lithium-content, dilute phases causes a more significant change in the rate of the increase in the graphite layer spacing compared with formation of high-lithium-content phases[34,40].

The asynchronous rate of stress and strain development with respect to potential (Fig. 4) leads to potential-dependent variations in stiffness. Interestingly, the evolution of the strain derivative (Fig. 4c) follows the current closely (Fig. 4a), indicating that the macroscopic strain developed in the composite electrode is correlated directly with changes in the graphite layer spacing at the atomic length scale as different graphite–lithium intercalation compounds are formed. In contrast, significant jumps in the stress derivative (Fig. 4b) precede any significant changes in strain for each of the phase transitions observed. For example, the increase in stiffness at 0.24 V shown in Fig. 3b is traced to a sharp increase in the rate of stress development with no corresponding increase in the rate of strain development. That is, stress develops before the active materials expand significantly.

The mechanical response of the electrode reported here contrasts with the conventional understanding of stress development in lithium-ion battery electrodes, which asserts that stress results from the expansion of the active material while the electrode is constrained, either globally by a substrate (that is, current collector) or locally by particle–particle interactions in a composite electrode[25]. Rather, our observation of the development of stress with minimal concurrent electrode expansion indicates that the mechanism of stress generation is more complex. The asynchronous development of stress and strain observed in Fig. 4 is the first indication that stress and strain responses in graphite electrodes are consequences of different but related time (kinetic)- and potential (thermodynamic)-dependent phenomena.

Figure 4d,e presents a schematic illustration of the proposed driving forces of stress and strain development that cause the stiffness increase at 0.24 V before the dilute stage I to stage IV transition. Since the stress is related to surface charge[41,42], we hypothesize that the increase of stress before the transition is caused by gradients in lithium-ion concentration that result from kinetic limitations on lithium-ion surface diffusion through the graphite microstructure[29,43–45]. Prior impedance studies on graphite electrodes reveal a sharp change in the lithium-ion diffusion coefficients at the phase transitions[29,30]. Interestingly, a large decrease in the Li diffusion constant was reported to occur just before the dilute stage I to stage IV transition[29], closely corresponding to the large change in stress (Fig. 4) and peak electrochemical stiffness (Fig. 3).

As lithium ions are inserted into the dilute stage I configuration, repulsive forces build between graphitic layers[34,46,47]. Once the repulsive forces reach a critical level, the stage IV phase is energetically preferable, and the transition is initiated[34,46,47]. Concurrent with the dilute stage I to stage IV transition, the graphite layer spacing increases and thus the macroscopic strain increases, leading to the decrease in the stiffness of the electrode. Similar considerations of stress developing before phase transitions and strain developing concurrent with phase transitions attend the other phase transitions.

We also evaluated the capacity-dependent mechanical response developed during galvanostatic cycling of graphite electrodes. Since galvanostatic cycling occurs at constant charge rate, the oscillations of the capacity-dependent stiffness occur within different phase transitions between graphite–lithium intercalation compounds relative to those seen during voltammetric cycling (see Supplementary Fig. 1). In cyclic voltammetry, the time spent per transition for the low-lithium-content transitions (that is, dilute stage I to stage IV) is longer relative to that in galvanostatic cycling.

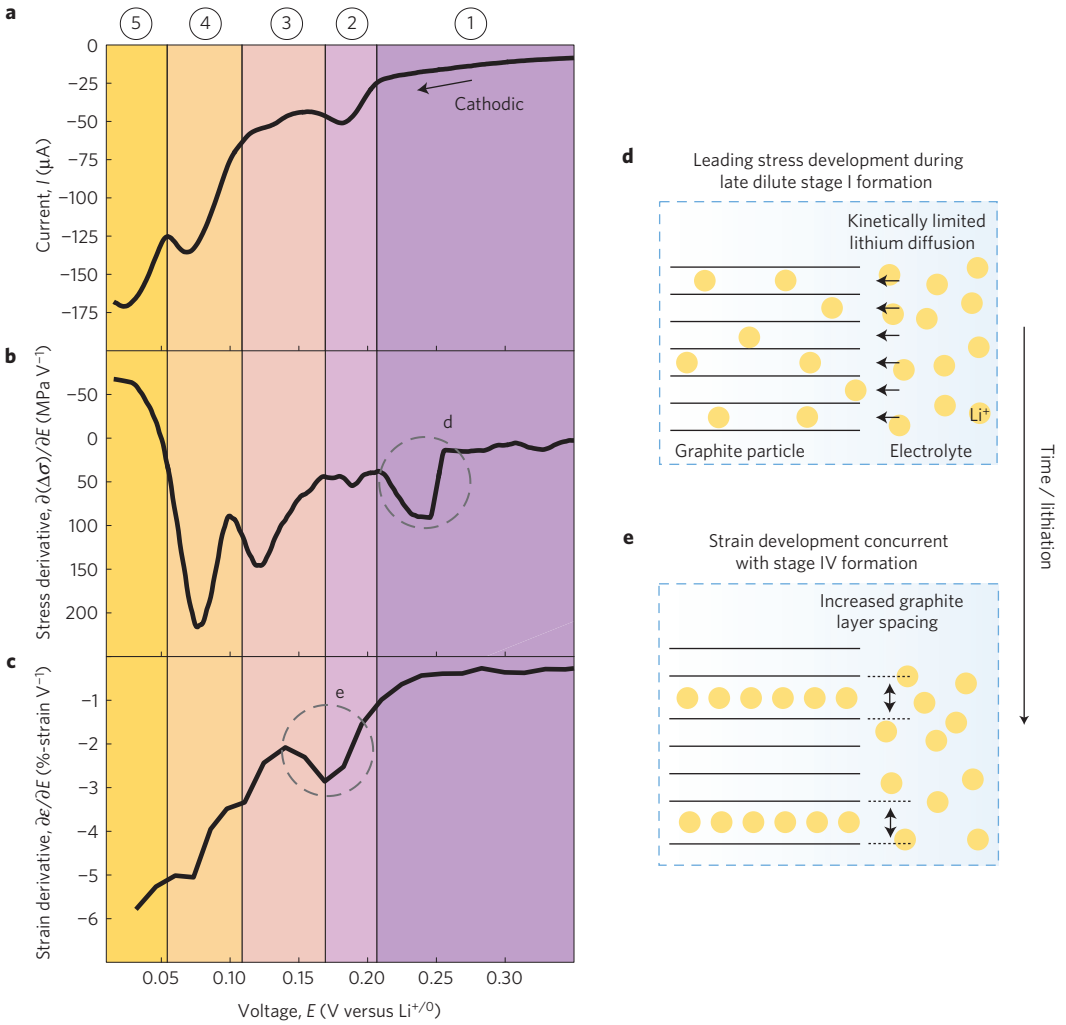

Figure 4 | Asynchronous development of stress and strain. a–c, Current response during the third cycle of cyclic voltammetry at 25 μV s^{-1} (Fig. 2a) (**a**) with corresponding rate of stress accumulation (**b**) and strain accumulation (**c**) during the cathodic sweep. The coloured regions correspond to phase transitions between graphite–lithium intercalation compounds: 1, formation of dilute stage I; 2, dilute stage I to stage IV, 3, stage IV to stage III to dilute stage II; 4, dilute stage II to stage II; 5, stage II to stage I. **d**, Schematic representation of leading stress developing at the end of the formation of dilute stage I (dashed circle in **b**). **e**, Schematic representation of strain developing concurrent with stage IV formation (dashed circle in **c**).

In contrast, the time spent per transition for the high-lithium-content transitions (that is, stage II to stage I) is much shorter. These different relative rates give rise to different stress and strain histories, which in turn change the appearance of the capacity-dependent stiffness compared with the potential-dependent stiffness. These results again suggest that time-dependent phenomena affect stress and strain development in electrodes differently.

Rate-dependent mechanical response

Intrigued by the asynchronous stress and strain development in the graphite electrodes, we explored the effect of intrinsic, materials-based rate limits on the stress and strain responses of graphitic electrodes. Figure 5 reports the current, capacity, stress-thickness, and strain responses of graphite composite electrodes during cyclic voltammetry at scan rates of 10 μV s^{-1}, 25 μV s^{-1} and 100 μV s^{-1}. Here, stress-thickness, the product of the stress in the electrode and the thickness of the electrode, is used instead of stress, since the active thickness of the electrode is unknown for the different scan rates. As expected, slower scan rate voltammetries exhibit more defined features corresponding to the lithium intercalation events, lower current magnitudes arising from slower lithiation rates (Fig. 5a), and higher specific capacities, that is, higher total lithium content[44,48] (Fig. 5b). Interestingly, the magnitude of the stress (Fig. 5c) correlates with the rate of lithiation, with both stress and current magnitudes decreasing with decreasing potential scan rate. In contrast, the strain development (Fig. 5d) correlates with the total lithium content, with both strain and capacity magnitudes increasing with decreasing scan rate. Thus, stress scales with current while strain scales with capacity. Most importantly, stress and strain scale inversely with respect to cycling rate, emphasizing that rate-dependent phenomena, such as diffusion of lithium ions, affect stress and strain differently.

When the cycling rate is slow and the rate of lithiation is slow (that is, the current magnitude is small), lithiation of the electrode is not limited by the diffusion rate of lithium in the graphite microstructure, and the stress is correspondingly small. In contrast, at a faster cycling rate, lithiation becomes diffusion-limited. The resulting gradient of lithium-ion concentration at the electrode surface causes higher stresses due to the slow diffusion[44,49,50] of lithium into the graphite microstructures.

The strain follows a different trend with cycling rate. During slow cycling, when lithiation is not diffusion-limited, lithium ions are able to diffuse through the electrode microstructure and fully lithiate the electrode, leading to a high specific capacity. The strain

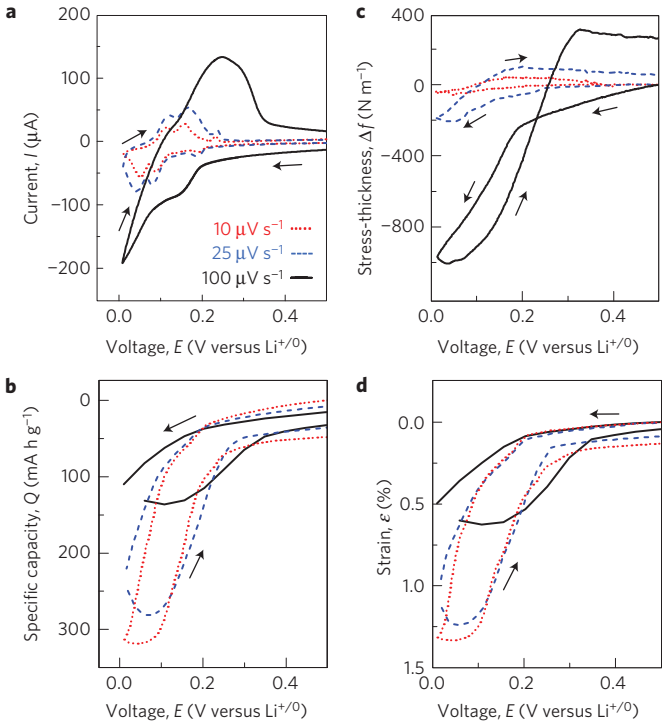

Figure 5 | Effect of the potential scan rate on the development of stress and strain in graphite electrodes. a–d, Current (**a**), specific capacity (**b**), stress-thickness (**c**) and strain (**d**) responses of graphite electrodes during the third cycle of cyclic voltammetry at 10 μV s^{-1}, 25 μV s^{-1} and 100 μV s^{-1}. For better comparison, stress and strain values of different scan rates are shifted to start from zero. The magnitude of stress scales with the current (that is, rate of lithium exchange) while the magnitude of strain scales with the specific capacity of the electrode (that is, total lithium content). Arrows represent the cathodic sweep (lithiation) as the voltage was decreased and the anodic sweep (delithiation) as the voltage was increased.

response follows the capacity response directly, and a larger strain is developed at a slower cycling rate. At faster cycling rates, the rate of lithium-ion transfer across the electrolyte/graphite interface becomes diffusion-limited, and the total charge intercalated into the electrode (specific capacity) is reduced. With fewer lithium ions inserted into the electrode, the strain response is also reduced.

Together, the potential and the rate dependence of the mechanical responses of graphite composite electrodes paint a complex picture of different but closely related time- and charge-dependent mechanisms that drive stress and strain development induced by lithium-ion exchange. Significant development of stress occurs when the lithiation rate is fast compared with the inherent diffusion rate of the electrode material, indicating a time-dependent, kinetically controlled process. Stress can develop even when few lithium ions are actually inserted into the electrodes. On the other hand, significant strain develops only when a sufficient amount of lithium ions have been inserted into the electrode. Thus, the strain response measures how many lithium ions have been inserted into the electrode, and is not sensitive to the rate of lithiation. Such time- and charge-dependent processes reveal intrinsic limits of electrode materials.

Conclusions

We have developed a new method to interrogate the mechanical response of battery electrodes. Combining coordinated, *in situ* measurements of stress and strain in battery electrodes enables us to calculate the electrochemical stiffness of lithium-ion battery electrodes. The electrochemical stiffness response reveals different stress and strain responses in graphite electrodes. Stress is governed by time-dependent, kinetically controlled lithium-ion insertion into the electrode while strain is governed by the amount of lithium inserted into the electrode. This stiffness response provides fundamental insight into rate behaviour possible from this and other battery materials. Diffusion limitations to the lithium insertion, manifested as a stiff electrode response, indicate a rate-limited material. To increase the intrinsic rate capability of electrode materials, lithium insertion needs to be more facile (for example, through improving surface diffusion), so that the stress and the strain develop more synchronously and electrochemical stiffness is lowered. This technique is applicable to any insertion-based material, the response from which will exhibit potential (thermodynamic)- and rate (kinetic)-dependent stiffnesses. Thus, the electrochemical stiffness response can be used to design and screen materials for battery electrodes for high-rate and -power applications.

Methods

Methods and any associated references are available in the online version of the paper.

Received 22 May 2015; accepted 20 June 2016; published online 1 August 2016

References

1. Etacheri, V., Marom, R., Elazari, R., Salitra, G. & Aurbach, D. Challenges in the development of advanced Li-ion batteries: a review. *Energy Environ. Sci.* **4,** 3243–3262 (2011).
2. Zaghib, K., Mauger, A., Groult, H., Goodenough, J. B. & Julien, C. M. Advanced electrodes for high power Li-ion batteries. *Materials* **6,** 1028–1049 (2013).
3. Tavassol, H., Cason, M. W., Nuzzo, R. G. & Gewirth, A. A. Influence of oxides on the stress evolution and reversibility during SnOx conversion and Li-Sn alloying reactions. *Adv. Energy Mater.* **5,** 1400317 (2015).
4. Tavassol, H. *et al*. Surface coverage and SEI induced electrochemical surface stress changes during Li deposition in a model system for Li-ion battery anodes. *J. Electrochem. Soc.* **160,** A888–A896 (2013).
5. Sethuraman, V. A., Chon, M. J., Shimshak, M., Srinivasan, V. & Guduru, P. R. *In situ* measurements of stress evolution in silicon thin films during electrochemical lithiation and delithiation. *J. Power Sources* **195,** 5062–5066 (2010).
6. Mukhopadhyay, A. *et al*. Engineering of graphene layer orientation to attain high rate capability and anisotropic properties in Li-ion battery electrodes. *Adv. Funct. Mater.* **23,** 2397–2404 (2013).
7. Chon, M. J., Sethuraman, V. A., McCormick, A., Srinivasan, V. & Guduru, P. R. Real-time measurement of stress and damage evolution during initial lithiation of crystalline silicon. *Phys. Rev. Lett.* **107,** 045503 (2011).
8. Mukhopadhyay, A., Tokranov, A., Xiao, X. & Sheldon, B. W. Stress development due to surface processes in graphite electrodes for Li-ion batteries: a first report. *Electrochim. Acta* **66,** 28–37 (2012).
9. Haiss, W. Surface stress of clean and adsorbate-covered solids. *Rep. Prog. Phys.* **64,** 591–648 (2001).
10. Sethuraman, V. A., Van Winkle, N., Abraham, D. P., Bower, A. F. & Guduru, P. R. Real-time stress measurements in lithium-ion battery negative-electrodes. *J. Power Sources* **206,** 334–342 (2012).
11. Mukhopadhyay, A., Tokranov, A., Sena, K., Xiao, X. & Sheldon, B. W. Thin film graphite electrodes with low stress generation during Li-intercalation. *Carbon* **49,** 2742–2749 (2011).
12. Eastwood, D. S. *et al*. Lithiation-induced dilation mapping in a lithium-ion battery electrode by 3D X-ray microscopy and digital volume correlation. *Adv. Energy Mater.* **4,** 1300506 (2014).
13. Ebner, M., Marone, F., Stampanoni, M. & Wood, V. Visualization and quantification of electrochemical and mechanical degradation in Li ion batteries. *Science* **342,** 716–720 (2013).
14. Huang, J. Y. *et al*. *In situ* observation of the electrochemical lithiation of a single SnO_2 nanowire electrode. *Science* **330,** 1515–1520 (2010).
15. Liu, X. H. *et al*. Anisotropic swelling and fracture of silicon nanowires during lithiation. *Nano Lett.* **11,** 3312–3318 (2011).
16. Jesse, S. *et al*. Direct mapping of ionic transport in a Si anode on the nanoscale: time domain electrochemical strain spectroscopy study. *ACS Nano* **5,** 9682–9695 (2011).
17. Balke, N. *et al*. Nanoscale mapping of ion diffusion in a lithium-ion battery cathode. *Nature Nanotech.* **5,** 749–754 (2010).

18. Lewis, R. B., Timmons, A., Mar, R. E. & Dahn, J. R. *In situ* AFM measurements of the expansion and contraction of amorphous Sn-Co-C films reacting with lithium. *J. Electrochem. Soc.* **154,** A213–A216 (2007).
19. Jones, E. M. C., Silberstein, M. N., White, S. R. & Sottos, N. R. *In situ* measurements of strains in composite battery electrodes during electrochemical cycling. *Exp. Mech.* **54,** 971–985 (2014).
20. Qi, Y. & Harris, S. J. *In situ* observation of strains during lithiation of a graphite electrode. *J. Electrochem. Soc.* **157,** A741–A747 (2010).
21. Ning, G., Haran, B. & Popov, B. N. Capacity fade study of lithium-ion batteries cycled at high discharge rates. *J. Power Sources* **117,** 160–169 (2003).
22. Buqa, H., Goers, D., Holzapfel, M., Spahr, M. E. & Novák, P. High rate capability of graphite negative electrodes for lithium-ion batteries. *J. Electrochem. Soc.* **152,** A474–A481 (2005).
23. Li, J., Murphy, E., Winnick, J. & Kohl, P. A. The effects of pulse charging on cycling characteristics of commercial lithium-ion batteries. *J. Power Sources* **102,** 302–309 (2001).
24. Li, Y. *et al*. Current-induced transition from particle-by-particle to concurrent intercalation in phase-separating battery electrodes. *Nature Mater.* **13,** 1149–1156 (2014).
25. Mukhopadhyay, A. & Sheldon, B. W. Deformation and stress in electrode materials for Li-ion batteries. *Prog. Mater. Sci.* **63,** 58–116 (2014).
26. Sethuraman, V. A., Hardwick, L. J., Srinivasan, V. & Kostecki, R. Surface structural disordering in graphite upon lithium intercalation/deintercalation. *J. Power Sources* **195,** 3655–3660 (2010).
27. Hardwick, L. J., Buqa, H. & Novák, P. Graphite surface disorder detection using *in situ* Raman microscopy. *Solid State Ion.* **177,** 2801–2806 (2006).
28. Barsoukov, E., Kim, J. H., Kim, J. H., Yoon, C. O. & Lee, H. Kinetics of lithium intercalation into carbon anodes: *in situ* impedance investigation of thickness and potential dependence. *Solid State Ion.* **116,** 249–261 (1999).
29. Funabiki, A. *et al*. Impedance study on the electrochemical lithium intercalation into natural graphite powder. *J. Electrochem. Soc.* **145,** 172–178 (1998).
30. Levi, M. D., Markevich, E. & Aurbach, D. The effect of slow interfacial kinetics on the chronoamperometric response of composite lithiated graphite electrodes and on the calculation of the chemical diffusion coefficient of Li ions in graphite. *J. Phys. Chem. B* **109,** 7420–7427 (2005).
31. Verma, P., Maire, P. & Novák, P. A review of the features and analyses of the solid electrolyte interphase in Li-ion batteries. *Electrochim. Acta* **55,** 6332–6341 (2010).
32. Xu, K. Electrolytes and interphases in Li-ion batteries and beyond. *Chem. Rev.* **114,** 11503–11618 (2014).
33. Tavassol, H., Buthker, J. W., Ferguson, G. A., Curtiss, L. A. & Gewirth, A. A. Solvent oligomerization during SEI formation on model systems for Li-ion battery anodes. *J. Electrochem. Soc.* **159,** A730–A738 (2012).
34. Dahn, J. R. Phase diagram of LixC6. *Phys. Rev. B* **44,** 9170–9177 (1991).
35. Aurbach, D., Levi, M. D., Levi, E. & Schechter, A. Failure and stabilization mechanisms of graphite electrodes. *J. Phys. Chem. B* **101,** 2195–2206 (1997).
36. Aurbach, D., Markovsky, B., Weissman, I., Levi, E. & Ein-Eli, Y. On the correlation between surface chemistry and performance of graphite negative electrodes for Li ion batteries. *Electrochim. Acta* **45,** 67–86 (1999).
37. Aurbach, D. *et al*. Common electroanalytical behavior of Li intercalation processes into graphite and transition metal oxides. *J. Electrochem. Soc.* **145,** 3024–3034 (1998).
38. Dresselhaus, M. S. & Dresselhaus, G. Intercalation compounds of graphite. *Adv. Phys.* **30,** 139–326 (1981).
39. Stevens, D. A. & Dahn, J. R. The mechanisms of lithium and sodium insertion in carbon materials. *J. Electrochem. Soc.* **148,** A803–A811 (2001).
40. Takami, N., Satoh, A., Hara, M. & Ohsaki, T. Structural and kinetic characterization of lithium intercalation into carbon anodes for secondary lithium batteries. *J. Electrochem. Soc.* **142,** 371–379 (1995).
41. Haiss, W. Surface stress of clean and adsorbate-covered solids. *Rep. Prog. Phys.* **64,** 591–644 (2001).
42. Haiss, W., Nichols, R. J., Sass, J. K. & Charle, K. P. Linear correlation between surface stress and surface charge in anion adsorption on Au(111). *J. Electroanalytical Chem.* **452,** 199–202 (1998).
43. Drozdov, A. D. A model for the mechanical response of electrode particles induced by lithium diffusion in Li-ion batteries. *Acta Mech.* **225,** 2987–3005 (2014).
44. Goodenough, J. B. & Park, K.-S. The Li-ion rechargeable battery: a perspective. *J. Am. Chem. Soc.* **135,** 1167–1176 (2013).
45. Van der Ven, A., Bhattacharya, J. & Belak, A. A. Understanding Li diffusion in Li-intercalation compounds. *Acc. Chem. Res.* **46,** 1216–1225 (2013).
46. Safran, S. A. Cooperative effects and staging n graphite intercalation compounds. *Synth. Met.* **2,** 1–15 (1980).
47. Dimiev, A. M. *et al*. Direct real-time monitoring of stage transitions in graphite intercalation compounds. *ACS Nano* **7,** 2773–2780 (2013).
48. Levi, M. D. & Aurbach, D. Simultaneous measurements and modeling of the electrochemical impedance and the cyclic voltammetric characteristics of graphite electrodes doped with lithium. *J. Phys. Chem. B* **101,** 4630–4640 (1997).
49. Persson, K. *et al*. Lithium diffusion in graphitic carbon. *J. Phys. Chem. Lett.* **1,** 1176–1180 (2010).
50. Zaghib, K., Song, X., Guerfi, A., Kostecki, R. & Kinoshita, K. Effect of particle morphology on lithium intercalation rates in natural graphite. *J. Power Sources* **124,** 505–512 (2003).

Acknowledgements

This work was supported by the Center for Electrochemical Energy Science, an Energy Frontier Research Center funded by the US Department of Energy, Office of Science, Basic Energy Sciences. E.M.C.J. acknowledges graduate fellowships through the National Science Foundation and the Beckman Institute for Advanced Science and Technology. The authors thank J. Lyding for use of spot welding equipment.

Author contributions

The manuscript was written through contributions of all authors. H.T. performed all stress measurements, E.M.C.J. performed all strain measurements and electrochemical stiffness calculations, and H.T. and E.M.C.J. jointly performed all data analysis. All authors contributed to interpretation of the data, and all authors have given approval to the final version of the manuscript.

Additional information

Supplementary information is available in the online version of the paper. Reprints and permissions information is available online at www.nature.com/reprints. Correspondence and requests for materials should be addressed to N.R.S. or A.A.G.

Competing financial interests

The authors declare no competing financial interests.

Methods

Graphite composite electrodes with a composition of 80 wt% graphite, 10 wt% carbon black, and 10 wt% polymer binder were fabricated. Electrodes for strain measurements were freestanding electrodes that were approximately 90–100 μm thick. Electrodes for stress measurements were fabricated on cantilever beams of passivated silicon. The silicon substrate was 250 μm thick and the graphite electrode was approximately 10 μm thick. Details of electrode fabrication are presented in the Supplementary Information.

Electrochemical cycling of the two types of graphite electrode was performed in independent custom battery cells against lithium metal counter electrodes, which has been described previously[4,19]. Cyclic voltammetry was performed at scan rates of 10 μV s^{-1} (1.00–0.01 V versus $Li^{+/0}$), 25 μV s^{-1} (1.00–0.01 V versus $Li^{+/0}$), and 100 μV s^{-1} (1.50–0.01 V versus $Li^{+/0}$) for three cycles. Galvanostatic measurements were performed at C/5 rate between 2 V and 0.01 V versus $Li^{+/0}$ for five cycles. Details of electrochemical measurements are presented in the Supplementary Information.

The stress-thickness (Δf) developed in the constrained electrode during electrochemical cycling was calculated from cantilever curvature changes using an optical set-up[4]. Stress values, $\Delta\sigma$, were calculated by normalizing the stress-thickness values by the thickness of the graphite electrode layer ($t_e = 10\,\mu m$) as $\Delta\sigma = \Delta f / t_e$. All stress-thickness values and stress values reported are changes in the values relative to the initial stress state of the pristine, as-fabricated electrode, which was unknown. The strain developed in the unconstrained electrode, ε, during electrochemical cycling was measured by using digital image correlation, an optical, non-contact, full-field strain measurement technique[19]. At the macroscopic length scale (about 2–4 mm), the composite electrode response was considered a homogeneous, isotropic average of the individual, anisotropic particle responses. The macroscopic stress state of the constrained electrode was therefore bi-axial compression or tension, and the average stress along the long axis of the cantilever is reported. The unconstrained electrode underwent free expansion and contraction isotropically, and the average strain along a line perpendicular to the long axis of the electrode is reported.

Stress and strain measurements obtained during cyclic voltammetry were correlated at each potential while stress and strain measurements obtained during galvanostatic cycling were correlated at each capacity. Details of the synchronization of the stress and strain measurements from independent but coordinated electrochemical experiments are presented in the Supplementary Information. The electrochemical stiffness was then calculated according to equation (1).